EXPERIMENTAL AND NUMERICAL INVESTIGATION OF NOISE GENERATION BY TURBULENT COMBUSTION IN A COMBUSTOR

S.R. Chakravarthy, S. Kartheekeyan, R.I. Sujith
Department of Aerospace Engineering
Indian Institute of Technology Madras
Chennai - 600 036, India
satya@aero.iitm.ernet.in, ae00m01@aero.iitm.ernet.in, sujith@iitm.ac.in

A. Sadiki, M. Düsing and J. Janicka
Chair of Energy and Powerplant Technology,
Department of Mechanical Engineering,
Darmstadt University of Technology,
Petersenstr. 30, 64287 Darmstadt, Germany
sadiki@ekt.tu-darmstadt.de, duesi@hrzpub.tu-darmstadt.de, janicka@ekt.tu-darmstadt.de

ABSTRACT

This paper is twofold. The first objective is to experimentally investigate the noise generated by combustion. For this purpose a turbulent air flow behind a rectangular half-dump combustor geometry is considered, with fuel injection just upstream of the dump plane. The fuel and air mix in the recirculation zone downstream of the dump plane, and the noise generated by the combustion is measured. The inlet flow Reynolds number is varied in the range of 15000-30000, and the overall fuel/air equivalence ratio is varied in the range 0.3-0.9. The observed total chemiluminescence intensity fluctuations are correlated with the noise spectra. The combustion noise exhibits a low frequency peak that is dominant when compared to the broadband diminished peak at the natural acoustic mode of the combustor. Secondly, LES calculations are presented for a rather simple configuration. To mimic some periodic phenomena in this configuration, LES computations are first performed using oscillating inflow conditions for predicting turbulent swirling methane-air diffusion flames. The influences of the inflow parameters on the scalar and velocity fields are presented and discussed.

INTRODUCTION

Noise generation in turbulent combustion systems could be a major problem in the context of gas turbine combustors in aircraft engine applications and in land-based gas turbines for power generation, among others (Strahle, 1978). In these systems the fluctuating density acts as a volume source of sound (the volume of the flame fluctuates with the reciprocal of the density). As pointed out by Klein (2000), the main cause for the fluctuating density are fluctuations in the heat release. The origin of these heat release fluctuations permits to distinguish between two phenomena. In the so-called combustion noise the density fluctuations are caused by autonomous turbulent fluctuations in the heat release. In the combustion driven oscillations or combustion instabilities the heat release of the flame depends on the acoustic phenomena in the combustion chamber due to a feedback loop between acoustics and combustion. The latter involves a complex interaction between unsteady heat release, the acoustic fluctuations and the vorticity field. In fact, unsteady heat release produces sound, which then generates (Kelvin-Helmholtz) waves at the inlet. These waves amplify and roll up on the shear layer and finally break down into small-scale motions, thereby affecting the heat release. The whole process forms then a closed loop (Schlüter, 2001). The phenomenon of combustion noise can be split up into the noise generation by the flame and the resonance in the combustion chamber. The object of many researchers in the past has been to model the chemical heat release distribution in order to predict the noise spectral shape and directionality (Clavin and Siggia, 1991; Boineau et al. 1996).

In recent times, computational fluid dynamics has been adopted for noise and combustion instability calculations. The long term objective of the present work aims to perform incompressible flow computations to evaluate the turbulent chemical heat release, and use this as the source term to predict the acoustic characteristics. Although such an approach has been adopted by a few authors in the recent past, their works have involved the RANS approach to the turbulence computations. Klein (2000) derived an integral equation that describes the sound spectrum as a function of the local turbulent mixture fraction spectrum at the flame front using information about the turbulence from a k-ε model. It is nowadays well recognized that Large Eddy Simulations (LES) are able to provide a detailed look at the dynamics of the large scale turbulent structures (their origin, development, and decay). LES can therefore deliver answers on how combustion noise and related instability phenomena modify the flow and scalar fields in the combustor. With regard to pollutant reduction and fuel efficiency many works have been oriented towards the control of combustion instability phenomena. While fully compressible simulations have been reported mainly for conditions where discrete frequencies prevail corresponding to excitation of instability-related mechanisms (for review, see Stone and Menon, 2001), in the present work incompressible (low Mach number) LES based computations are performed using the infinitely fast chemistry and the mixture fraction formalism for determining the heat release. To mimic some periodic phenomena, we reduce the described effects in considering oscillating conditions at the inlet and look at their influences on scalar and velocity fields.

Experimentally, investigations are carried out to measure the acoustic pressure level and estimate the heat release fluctuations by means of high-speed chemiluminescence imaging of the combustion zone (Ramohalli et al., 1984). These

results will be used to validate LES evaluations of the turbulent chemical heat release and the acoustic pressure in the future.

EXPERIMENTAL DETAILS

The geometry adopted in the present work is shown in Figure 1. It is a half-dump combustor with a rectangular test section and the fuel injection just upstream of the dump plane. Commercially available liquid petroleum gas (LPG), containing approximately 90% butane and 10% propane, was used in the experiments. The fuel-air mixing occurs in the recirculation zone downstream of the dump plane. Windows are provided in this region of the experimental set-up for optical access to image the chemiluminescent intensity fluctuations in a time-resolved manner with the help of a high-speed digital CCD camera. The framing rate adopted in the experiments is 2250 frames per second. Acoustic pressure is measured at a port just downstream of the bottom of the dump plane with a piezo-electric transducer mounted on an air-cooled probe. Adequate calibration is made to account for the air-cooled probe over the entire frequency range of interest. The acoustic pressure data is acquired with the help of an A/D converter at a sampling rate of 10000 Hz for 1 second duration. The flow Reynolds number based on the hydraulic mean diameter of the inlet of the test section and the average velocity at the inlet section is varied in the range 15000-30000. Mesh screens are provided at the inlet of the set-up to ensure uniform turbulence intensity levels. Experiments have been performed for the overall equivalence ratio in the range 0.3-0.9. The flow rates of air and fuel are measured by means of rotameters with errors within 2%. Repeatability of the acoustic results is observed to be within 5%.

EXPERIMENTAL RESULTS

Acoustic Pressure Measurements

Figure 2 shows the acoustic spectra with variation in the air flow Reynolds number and the overall equivalence ratio. It can be seen that under all conditions, the spectra show broadband peaks mainly at two frequencies, namely, around 60-80 Hz, and around 600 Hz; the former is sharper than the latter. It corresponds to the natural vortex shedding frequency of the large scale eddies, and correlates with a Strouhal number of around 0.2 based on the height of the dump plane, and the average velocity at the combustor inlet, in the test range of Reynolds numbers. The latter peak corresponds to the natural acoustic mode of the duct, approximately with open boundary conditions at both ends. A minor broadband peak at around 1400 Hz is also seen for the equivalence ratio of 0.9, corresponding to a harmonic of the natural acoustic mode. The fact that the first two peaks are far apart indicates that the mechanism of sound generation is mainly related to noise and not as much related to feedback-based instability; combustion noise is also a low-frequency phenomenon. The peak corresponding to the vortex shedding frequency being the dominant supports the understanding that the noise is generated by the energy containing eddies. Regarding the amplitudes, it can be seen that the pressure level roughly increases proportionately to increase in the flow Reynolds number, but is relatively insensitive to the equivalence ratio. The former trend, unlike the latter, is not in conformance with trends reported in the literature for open flames.

Chemiluminescent Intensity Fluctuations

Fourier transforms of the time variation of the total intensity of chemiluminescence from the combustion zone has been obtained under the test conditions. The total chemiluminescent intensity is a good indication of the volume-integrated chemical heat release, considering the line-of-sight integration of the chemiluminescence intensity in the two-dimensional setup adopted in the present study. Figure 3 shows waterfall plots of the total chemiluminescent intensity spectra as a function of the overall equivalence ratio at different flow Reynolds numbers. A peak at nearly zero frequency can be seen in some of the spectra, indicating a strong mean heat release over the imaging time. Disregarding this, the figure shows that the peak of the oscillatory heat release consistently spreads around 60-80 Hz. Smaller peaks are also seen at about twice this frequency. These frequencies are related to the large-scale vertical structures in the turbulent recirculation zone downstream of the dump plane, and due to the break up of these structures further downstream. Looking at the high-speed chemiluminescence images (not shown here in the interest of brevity), the vortical structures are quite evident, indicating the intense vortex combustion that occurs in the turbulent recirculation zone. The amplitudes of the total chemiluminescent intensity fluctuations show a decrease with increasing flow Reynolds number, but expectedly increase with increasing the overall equivalence ratio. The absence of peaks in the total chemiluminescent intensity fluctuations at the duct natural modes confirms a lack of acoustic feedback on the combustion process.

As seen before, the duct natural acoustic mode is removed far from the driving frequency from the total heat release fluctuations. However, the decrease in the intensity fluctuations amplitude with increase in Reynolds number is the reverse of the trend exhibited by the acoustic pressure. Recall that the acoustic pressure is measured at the dump plane, but the flame is stabilized at a significant distance (2-3 dump plane heights) from the dump plane. This shows that the vortex shedding in the recirculation zone dominates the pressure fluctuation, with the combustion amplifying it. The latter point is evident if one considers the cold flow acoustic pressure amplitudes, which are lower than their corresponding hot flow amplitudes by an order of magnitude. The sensitivity of the chemiluminescent intensity to the overall equivalence ratio indicates good mixing enabled by the turbulent vortices.

NUMERICAL DETAILS

In order to evaluate the performance of LES in predicting effects of combustion noise, we first perform LES of turbulent swirling diffusion flames with oscillating inflow conditions in a rather simple model combustor. Methane is used as fuel instead of LPG.

Computational Domain and Boundary Conditions

The axissymetric computational domain shown in figure 4 is discretised by a structured staggered grid ($n_1 \times n_2 \times n_3 = 193 \times 64 \times 30 \Rightarrow 370\,560$ cells). It describes a cylindrical combustion chamber with two coaxial inflow nozzles. In nozzle N_1, the axial velocity of methane is set to the mean value, superimposed with a harmonically oscillating signal and random noise (figure 5). This results in a fuel air ratio of $\phi = 0.5$. The radial and tangential velocity components consist of random noise only. The inflow conditions on the outer nozzle N_2

drive the air flow in axial and tangential (swirl) directions. Random noise is added to the mean flow velocity. Boundary conditions for pressure and velocity are summarized in table 1. Other simulation parameters are given in table 2.

Table 3 shows the main parameters of the performed simulations. In these tables, $\mathbf{n}$, p, P_{therm}, T, f and $\omega = 2\,\pi\,f$ denote the unit vector normal to the boundary, pressure, thermal power of the burner, temperature, frequency and angular frequency, respectively. The subscripts $(\cdot)_{out}$ and $(\cdot)_w$ denote quantities at the outflow and at the wall respectively. $\widehat{u}_{1,N_1}/\overline{u}_{1,N_1}$ denotes the normalized amplitude of the oscillation and u_i' is the random noise (see also figure 5).

Numerical Procedure

Simulations are carried out using a Large Eddy Finite Volume Code. The equations are integrated in time by a 3rd order low-storage Runge-Kutta scheme. Pressure is determined by solving a Poisson equation derived from the equation of continuity. The density varies in space and time, but it is assumed to be independent from pressure (Low Mach-number assumption, incompressibility). Therefore, the term $\partial\overline{\rho}/\partial t$ appears as a source term in the Poisson equation. The momentum subgrid closure is realized by the Smagorinsky model together with the dynamic Germano procedure (Lilly, 1992).

Following Forkel and Janicka (1999), the chemical composition is described by solving the filtered transport equation for $\overline{\rho F}$.

$$\frac{\partial\left(\overline{\rho F}\right)}{\partial t}+\frac{\partial\left(\overline{\rho}\,\widetilde{F}\,\widetilde{u}_j\right)}{\partial x_j}=\frac{\partial}{\partial x_j}\left(\frac{\overline{\rho}\,(\widetilde{\nu}+\nu_t)}{\sigma}\frac{\partial\,\widetilde{F}}{\partial x_j}\right) \qquad (1)$$

In equation (1) ρ, F, u_i, ν, ν_t and σ denote the density, mixture fraction, velocity, molecular viscosity, turbulent viscosity and Schmidt-Number, respectively. $\overline{(\cdot)}$ denotes a filtered quantity, while $\widetilde{(\cdot)}$ expresses a Favre-filtered quantity. Mixture fraction is set by definition to unity for pure methane and zero for pure air. Time integration of eq. (1) yields $\overline{\rho F}$, not $\widetilde{F}$. Hence, in order to determine $\overline{\rho}$ and $\widetilde{F}$, for every timestep and grid cell, a non-linear equation has to be solved. Unfortunatelly, there exist up to three solutions to this equation. In order to find the physically correct one, all solutions for $\widetilde{F}$ are determined. Then (assuming steady changes) the one closest to the value of the last timestep is chosen. Assuming chemical equilibrium, density, molecular viscosity, temperature, and species mass-fractions are evaluated as functions of the Favre-filtered mixture fraction $\widetilde{F}$ and its subgrid variance $\widetilde{F''^2}$. The latter is approximated by the resolved variation in a domain twice the size of a grid cell. The subgrid distribution of $\widetilde{F}$ is modelled with the use of a β-function. To ensure stability, $\overline{\rho}$ is relaxed in time . A detailed description of the numerical procedure can be found in Kempf et al. (2000).
In order to calculate the sound spectrum, an expression of the sound pressure as function of the heat release will be needed. Assuming chemical equilibrium, the heat release will be expressed as function of the mixture fraction.

NUMERICAL RESULTS

As well known, LES depends strongly on the inflow conditions. It is therefore interesting to not only capture the imposed frequencies, but to also predict their influence on the flow and scalar fields.

Prediction of excited frequencies

To analyze the influence of oscillating inflow conditions on the flow field, we applied the Fourier transform in time to the velocity data. Because there is a link between a statistically-stationary periodic process, its spectral representation (in terms of Fourier modes), its power spectrum and its autocorrelation function, only the turbulent spectrum $\mathcal{E}_i(f)$ evaluated with respect to the equally spaced data (Δt) is presented. In figure 6, the $f^{-5/3}$ power law can be retrieved as well as the excitation frequency of $f = 800\,Hz$. The autocorrelation functions (not shwon) oscillate with the imposed frequencies. An analysis of the pressure distribution obtained from the Poisson equation presented in figure 7 also allows to clearly retrace the imposed frequency.

To calculate the sound spectrum, the Fourier transform in time of the correlation function of the expression of the sound pressure as function of the heat release is needed. Assuming chemical equilibrium, the heat release can be expressed as function of the mixture fraction. It is instantaneous and given at the position of the flame front mainly determined by the large scale mixing of fuel and air. It depends among others on the scalar dissipation which is the irreversible fine scale mixing by molecular diffusion (scalar dissipation). Although these parameters can be well derived from the CFD calculations, the spectrum of the pressure fluctuations due to combustion could not yet be provided at the stage of the investigation.

Amplitude of the forced frequencies in reacting and non-reacting non-swirling cases

For non-swirling flows, the influence of the imposed frequency is often more impressive. Figure 8 shows peak values of the imposed frequencies determined from Fourier transformation at different axial positions of the flow field. The case without excitation (0 Hz) is used for comparison[1]. In cases without reaction (200, 400 and 1600 Hz) and for $x_1 \leq 650\,mm$, amplitudes are high compared to the non-excited case. For $x_1 \geq 650\,mm$, the amplitudes nearly have fallen to the value of case without excitation, indicating that the imposed frequency cannot be detected in this region. Especially in the 200 Hz case and in the reacting case (see case 4 in tab. 3), calculated with the same smaller amplitudes of the excitation, lower values compared to non-reacting cases with 400 and 1600 Hz (amplitude: 0.1) occur close to the nozzles. One clearly finds that frequencies die out slowly with increasing distance from the inflow, and that lower frequencies (see case with 400 Hz) penetrate further into the flow field than higher frequencies (case with 1600 Hz). The details about the simulation for non-reacting cases can be found in Düsing et al. (2002).
For case with reaction (case 4), the oscillation seems to vanish earlier than in cases without reaction.

Flow and scalar fields

Concerning the influence of the oscillating inflow on flow fields, the results actually confirm the findings by Weinberger et al. (1997). The mean flow quantities like the normalized mean axial profiles and the spreading rate are

[1] Due to the fact that no imposed frequency exists, an arbitrary frequency has to be chosen (here: $f = 400\,Hz$)

almost independent of the inlet conditions, while the mean profile of the inlet velocity has only a minor influence on the near field. Düsing et al. (2002) showed however, that the turbulence characteristics are considerably influenced. This is the reason why the simulations with reaction are more affected by the excitation frequencies than those without reaction.

Assuming the infinitely fast chemistry, the combustion processes are dominated by the mixing of the fuel and air streams, which in turn is determined by the state of turbulence. It is then interesting to display the influence of the oscillating inflow conditions on scalar fields. In particular, figure 9 shows the mean temperatures for two swirled methane-air cases (1 and 2). These profiles show considerable differences, indicating a displacement of the flame to higher radii. Moreover, the flattened temperature profiles of the cases with oscillating inflow conditions compared to those without implies a more effective mixing.

CONCLUSIONS

From the experimental part of this work, correlated volume-integrated heat release rate with acoustic pressure data have been provided using the digital image processing of the high-speed chemiluminescent images. The combustion noise could be characterized as a low frequency phenomenon. LES performs very well in predicting 1) interesting features of the oscillating velocity inflow conditions, in particular the frequencies imposed, 2) the influence of these conditions on the mean temperature.
The task of calculating the fluctuating chemical heat release rate and the acoustic pressure as well as the comparison with experiments has been left for future work.

ACKNOWLEDGMENTS

This work has been initiated during the stay of the first author at the TU-Darmstadt. The authors are grateful for the financial support by the DFG Forschergruppe "Verbrennungslärm" and the DFG-Sonderforschungsbereich 568 "Strömung und Verbrennung in zukünftigen Gasturbinenbrennkammern".

REFERENCES

Boineau, P., Gervais, Y. and Morice, V., 1996, "An Aerothermoacoustic Model for Computation of Sound Radiated by Turbulent Flames," Proceedings of Internoise, Vol. 96, pp. 495-498.

Clavin, P. and Siggia, E. D., 1991, "Turbulent Premixed Flames and Sound Generation," Combustion Science and Technology, Vol. 78, pp. 147-155.

Düsing, M., Hauser, A., Sadiki, A. and Janicka, J., 2002," LES of confined methane-air diffusion flames using oscillating inflow conditions," Engineering Turbulence Modelling and Experiments - 5, W. Rodi and N. Fueyo (Ed), pp. 917-926, Elsevier Sc. Ltd.

Forkel, H. and Janicka, J., 1999, "LES of a turbulent hydrogen diffusion Flame," TSFP-1, Boulder, USA

Kempf, A., Forkel, H., Sadiki, A., Janicka, J. and Chen, J.-Y., 2000, "Large-Eddy Simulation of a Counterflow Configuration with and without Combustion," Proc. Combust. Inst. 28th Conf., 35-40

Klein, S., 2000, On the Acoustics of Turbulent Non-Premixed Flames," Ph.D. Thesis, University of Twente, Enschede, The Netherlands.

Lilly, D.K., 1992, "A proposed modification of the Germano subgrid-scale closure method," Physics of Fluids A, 4:633-635

Ramohalli, K. and Seshan, P., 1984, "Acoustic Imaging for Local Diagnostics of Chemically Reacting Systems," Combustion Science and Technology, Vol. 37, pp. 253-261.

Stone, C. and Menon, S., 2001b, "Combustion Instabilities in Swirling Flows," AIAA Paper No. 2001-3846.

Strahle, W. C., 1978, "Combustion Noise," Progess in Energy and Combustion Science, Vol. 4, No. 3, pp. 157-176.

Schlüter, J. U., 2001, "Large-eddy simulations of combustion instability suppression by static turbulence control," Annual Research Briefs 2001, pp 119-130, CTR, Stanford University, USA

Weinberger, C., Rewerts, J. and Janicka, J., 1997, "The influence of inlet conditions on a large eddy simulation of a turbulent planar jet", 11th Symp. on Turbulent Shear Flows, Grenoble, France

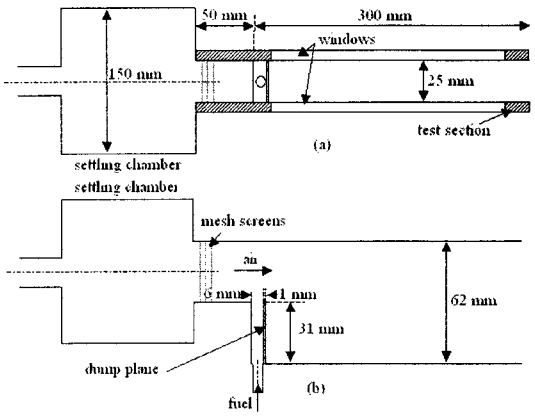

Figure 1: Schematic of the experimental set-up: (a) top view, (b) front view.

Table 1: Boundary Conditions

Pressure	
Inflow, wall	$\partial \overline{p}/\partial \mathbf{n} = 0$
Outflow	$\overline{p} = p_{out} = const.$
Velocity	
Nozzle: N_1	$u_{1,N_1}(\mathbf{x},t) = \overline{u}_{1,N_1} + \widehat{u}_{1,N_1}\ \sin(\omega\, t) + u'_{1,N_1}$
	$u_{2,N_1}(\mathbf{x},t) = u'_{2,N_1}$; $\quad u_{3,N_1}(\mathbf{x},t) = u'_{3,N_1}$
Nozzle: N_2	$u_{1,N_2}(\mathbf{x},t) = \overline{u}_{1,N_2} + u'_{1,N_2}$;
	$u_{2,N_2}(\mathbf{x},t) = \overline{u}_{2,N_2} + u'_{2,N_2}$
	$u_{3,N_2}(\mathbf{x},t) = u'_{3,N_2}$
Wall	$u_{i,w}\ (\mathbf{x},t) = 0$
Outflow	$\partial\, u_{i,out}/\partial \mathbf{n} = 0$

Table 2: General simulation parameters

ϕ	P_{therm}	T_{N_1}	T_{N_2}	p_{out}	$\overline{u}_{1,N_{1,2}}$	$\overline{u}_{2,N_2}$
0.5	17.5	300	773	30	50	35
–	MW	K	K	bar	m/s	m/s

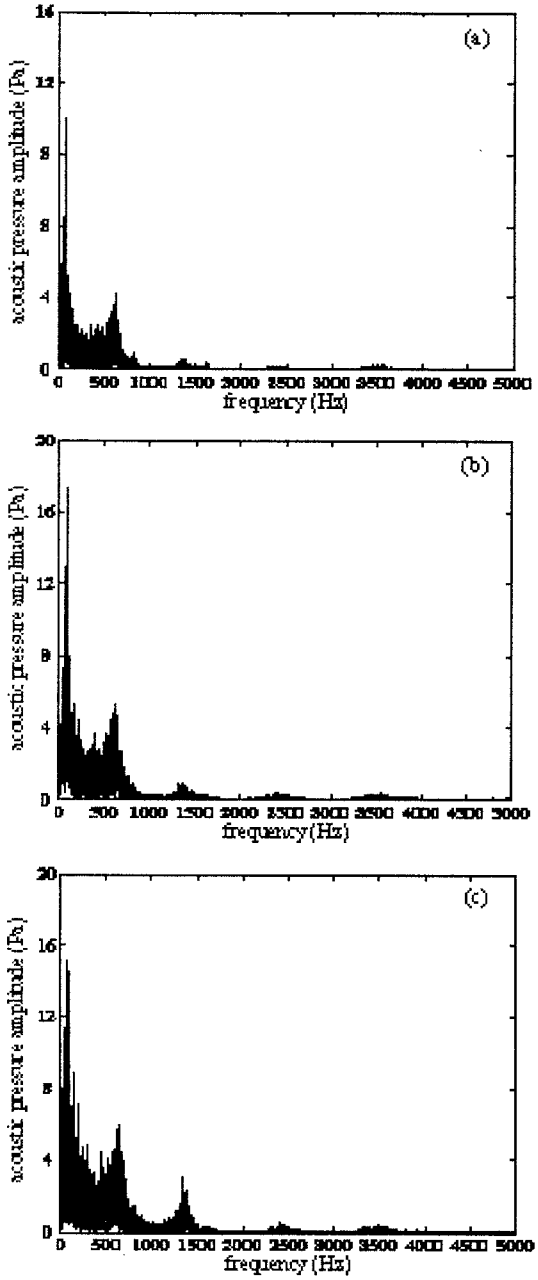

Figure 2: Acoustic pressure spectra at the dump plane with (a) $Re = 20020$ and $\phi = 0.4$, (b) $Re = 25625$, $\phi = 0.4$, and (c) $Re = 25625$, $\phi = 0.9$.

Table 3: Performed simulations (methane-air-chemistry)

case	frequency f	amplitude $\widehat{u}_{1,N1}/\overline{u}_{1,N1}$	swirl
1	0 Hz	-	yes
2	200 Hz	0.1	yes
3	800 Hz	0.1	yes
4	800 Hz	0.025	no

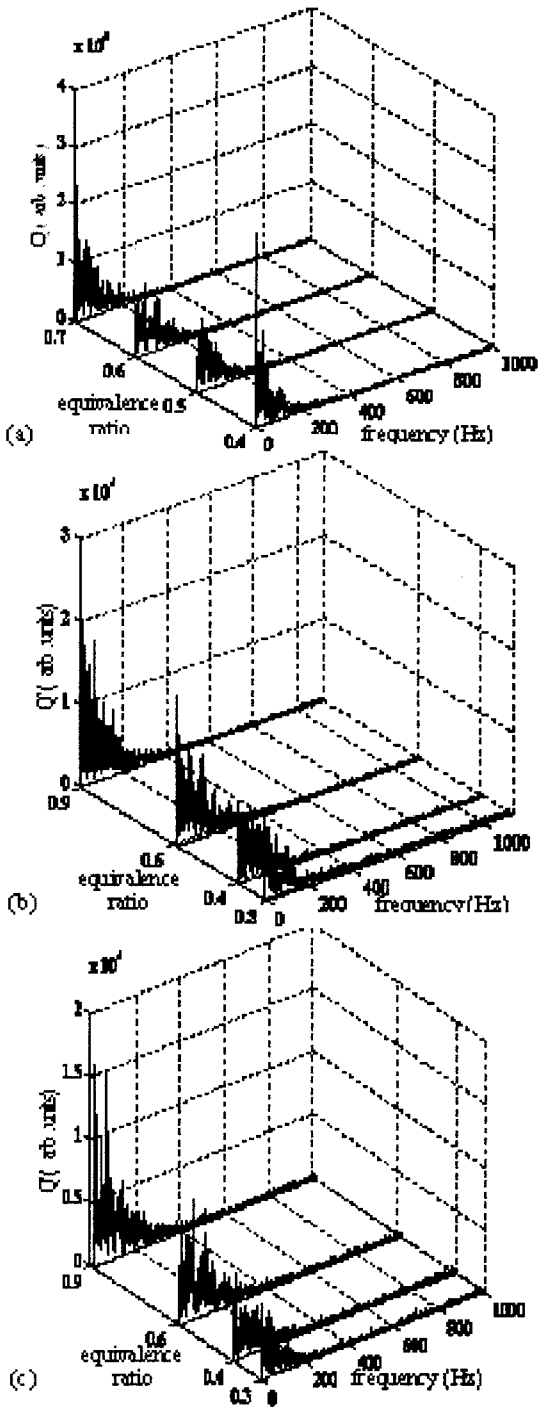

Figure 3: Total chemiluminescent intensity spectra as a function of equivalence ratio at different Reynolds number: (a) 20020, (b) 25625, (c) 30430.

Figure 4: Computational domain

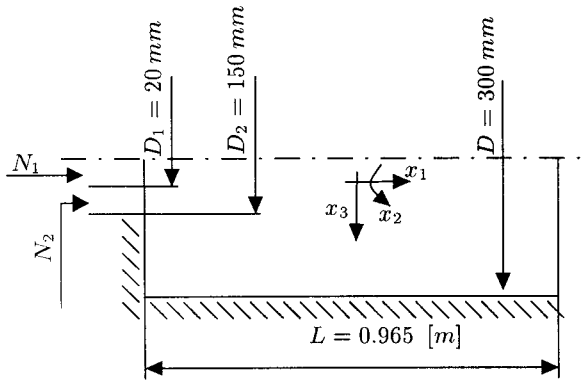

Figure 5: Sketch of the imposed inflow oscillations

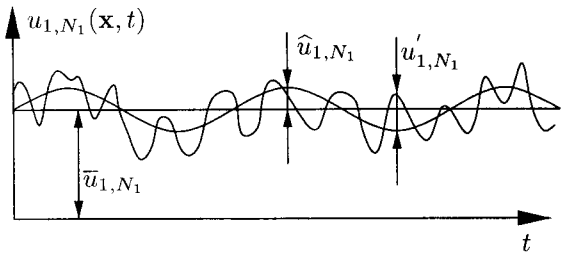

Figure 6: Power spectrum of the u_3-velocity at $x_1 = 60\,mm$, $x_3 = 100\,mm$ for case 3. A dashed $f^{-5/3}$-line has been added.

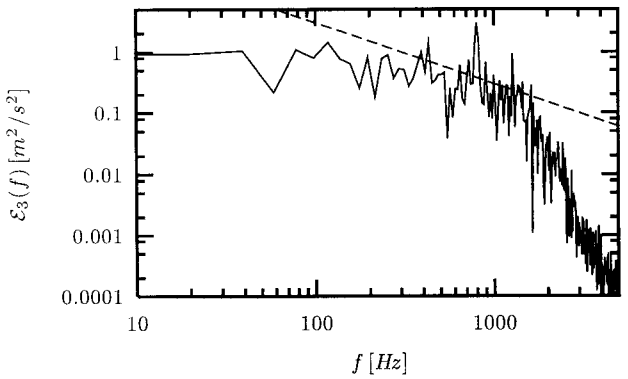

Figure 7: Fourier Analysis of the pressure distribution ($r = 50\,[mm]$ and $x = 180\,[mm]$)

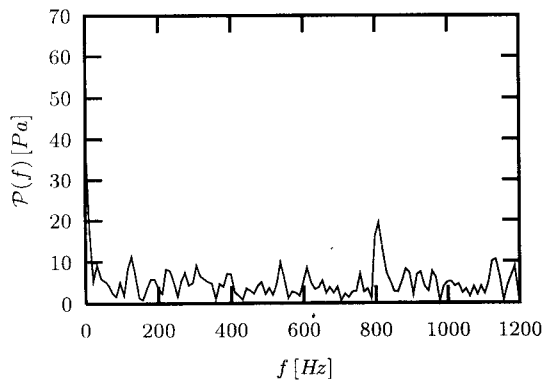

Figure 8: Amplitudes of the forced frequencies along the axis: thick line for case 4; the other lines for non-reacting (air-air) simulations with 0 (thin), 200 (dashed), 400 (small dashed) and 1600 (dashed-dotted)

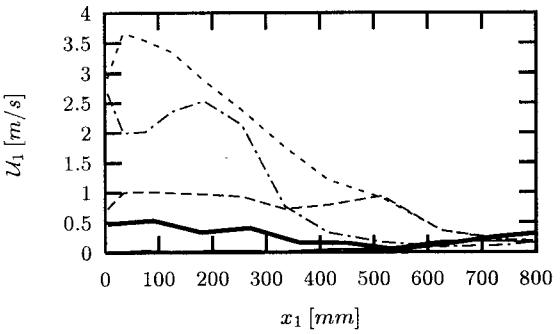

Figure 9: Mean temperatures for case 1 (thin) and case 2 (thick) at different axial positions